Shape Control in Iron Oxide Nanocrystal Synthesis, Induced by Trioctylammonium Ions

Alexey Shavel,*,† Benito Rodríguez-González,† Jessica Pacifico,† Marina Spasova,‡ Michael Farle,‡ and Luis M. Liz-Marzán*,†

Departamento de Química Física and Unidad Asociada CSIC, Universidade de Vigo, 36310 Vigo, Spain, and Fachbereich Physik and Center for Nanointegration (CeNIDE), Universität Duisburg-Essen, Lotharstrasse 1, 47048, Duisburg, Germany

Received November 26, 2008. Revised Manuscript Received January 21, 2009

Faceted iron oxide nanoparticles with octahedral shape were synthesized through controlled modification of the iron oleate decomposition method. The key to this novel shape control is the "in situ" formation of trioctylammonium bromide (TOAHB) during the process, through decomposition of quaternary ammonium salts. This hypothesis was confirmed by carrying out the synthesis in the presence of preformed TOAHB, which again resulted in the formation of iron oxide octahedra. A detailed high-resolution transmission electron microscopy (HRTEM) analysis of the nanooctahedra was performed for shape analysis and structural characterization. X-ray photoelectron spectroscopy (XPS) indicates the presence of both metallic iron and iron oxide within the nanooctahedra. The results obtained by HRTEM and XPS are in agreement with magnetic analysis, which revealed the presence of several magnetic phases in the samples.

Introduction

Shape control is one of the most exciting challenges within chemical nanotechnology, mainly because the interesting properties of nanomaterials can be tuned through variations in their morphology, but also because assembly is strongly affected. An extended overview on the shape-selected synthesis of inorganic nanoparticles has been recently published.[1] Although significant progress has been made for a number of metals and metal oxides, shape control of the most interesting iron oxides (magnetite, maghemite) is not well developed. Apart from the most common spherical shape, iron oxide nanocrystals with cubic,[2,3] tetrapod,[4] tubular (with parallelogram cross-section),[5] and pyramidal[2] shapes have been published. Additionally, mixtures of spherical-, triangular-, and diamond-shaped iron oxide nanocrystals were obtained by injection of iron pentacarbonyl into a solution of dodecylamine in dichlorobenzene.[6] The synthesis of iron oxide octahedra with average particle size around 50 nm in aqueous medium was recently reported,[7] though the achieved size distributions were rather wide and detailed analysis of the nanoparticles structure was not provided. At the same time, the mechanism underlying the formation of various different shapes for iron oxide nanoparticles is still unclear.

The role of the different components within the reaction mixture on the specific growth mechanism of various types of nanoparticles has been only studied in detail for certain synthetic processes. However, particularly when the synthesis is performed in organic solvents, the role of the various chemical reactions that can occur involving the organic components present in the reaction medium during the preparation of inorganic nanoparticles is still underestimated. In fact, a number of different organic reactions can take place during the thermolytic decomposition of organometallic precursors, because the organic components of the reaction mixture can undergo different chemical reactions at the high temperature that is usually employed for the synthesis of high-quality iron oxide nanoparticles. Unfortunately, this problem has only been briefly addressed.[8]

In the particular case of iron oxide formation from iron oleate complex, sodium oleate ionization can take place at elevated temperature, leading to the "in situ" production of relevant reactants−surfactants. Organic solutions of alkaline metal oleates become conductive at high temperatures, yielding the corresponding alkaline cations and oleate at about 200 °C. Oppositely, pure oleic acid is stable under similar conditions. Using this reaction (production of oleate anions), the syntheses of iron oxide[2] and iron@iron oxide[3]

* Fax: (+34)986812556. E-mail: shavel@uvigo.es (A.S.); lmarzan@uvigo.es (L.M.L.-M.).
† Universidade de Vigo.
‡ Universität Duisburg-Essen.

(1) Jun, Y.-W.; Choi, J.-S.; Cheon, J. *Angew. Chem., Int. Ed.* **2006**, *45*, 3414–3439.
(2) Kovalenko, M. V.; Bodnarchuk, M. I.; Lechner, R. T.; Hesser, G.; Schaffler, F.; Heiss, W. *J. Am. Chem. Soc.* **2007**, *129*, 6352–6353.
(3) Shavel, A.; Rodríguez-González, B.; Spasova, M.; Farle, M.; Liz-Marzán, L. M. *Adv. Funct. Mater.* **2007**, *17*, 3870–3876.
(4) Cozzoli, P. D.; Snoeck, E.; Garcia, M. A.; Giannini, C.; Guagliardi, A.; Cervellino, A.; Gozzo, F.; Hernando, A.; Achterhold, K.; Ciobanu, N.; Parak, F. G.; Cingolani, R.; Manna, L. *Nano Lett.* **2006**, *6*, 1966–1972.
(5) Yu, T.; Park, J.; Moon, J.; An, K.; Piao, Y.; Hyeon, T. *J. Am. Chem. Soc.* **2007**, *129*, 14558–14559.
(6) Cheon, J.; Kang, N.-J.; Lee, S.-M.; Lee, J.-H.; Yoon, J.-H.; Oh, S. J. *J. Am. Chem. Soc.* **2004**, *126*, 1950–1951.
(7) Vereda, F.; de Vicente, J.; Morales, M. d. P.; Rull, F.; Hidalgo-Alvarez, R. *J. Phys. Chem. C* **2008**, *112*, 5843–5849.
(8) Garnweitner, G.; Niederberger, M. *J. Mater. Chem.* **2008**, *18*, 1171–1182.

10.1021/cm803201p CCC: $40.75
Published on Web 03/06/2009

nanocubes have been reported. According to ref 2, nanoparticles with pyramidal shape can also be prepared. A crucial point in this process is that when exclusively oleic acid is present in the reaction mixture, the growth of faceted nanoparticles with cubic or pyramidal shape is prevented. Therefore, using pure oleic acid as a stabilizer has become a standard procedure for the preparation of high-quality, spherical maghemite nanoparticles.

In this paper, we explored the possibility of influencing nanoparticle growth through either direct addition of trioctylammonium bromide (TOAHB) or "in situ" decomposition of tetraoctylammonium bromide (TOAB). The presence of TOAHB leads to the formation of strongly faceted iron oxide nanocrystals, with well-defined octahedral shape. Interestingly, detailed structural characterization and XPS analysis demonstrate the presence of metalic iron-rich areas inside these maghemite nanooctahedra, which is also reflected in their magnetic response.

Experimental Section

All reagents were used as received without further purification.

Preparation of the Iron Oleate Complex. The iron precursor (iron oleate complex) was synthesized as follows: 1.298 g (8 mmol) of $FeCl_3$ (Aldrich, 97%) and 7.3 g (24 mmol) of sodium oleate (TCI, 95%) were dissolved in a mixture of water (12 mL), ethanol (16 mL), and hexane (28 mL). The resulting mixture was stirred overnight at room temperature. The upper organic black layer was separated and washed 5 times with hot (60 °C) deionized (Milli-Q) water in a separating funnel (washing with hot water reduced sodium content below the sensitivity of XPS) and dried under a stream of argon first at 60 °C (to remove hexane) and finally at 120 °C. The resulting iron−oleate complex is a viscous, waxy brown liquid. Careful control of the iron/sodium oleate ratio is necessary as a small excess of sodium oleate may have a marked influence on the shape of the particles.[3]

Preparation of Trioctylammonium Bromide (TOAHB). Trioctylamine (8.84 g, 25 mmol; TOA; Aldrich 98%) was dissolved in 30 mL of hexane, and 4.3 g (43 wt % in H_2O) of HBr solution was added dropwise under strong stirring. When the reaction was completed, the organic phase was extensively washed with Milli-Q water. Upon evaporation of hexane (in a rotary evaporator), a white powder of trioctylammonium bromide was obtained.

Preparation of Fe_xO_y Octahedra. The iron oxide nanocrystals were synthesized according to the following procedure. 0.9 g (1 mmol) of iron oleate complex, an appropriate amount of tetraoctylammonium bromide (TOAB; Fluka, >98%) or premade TOAHB and 141 mg (0.5 mmol) of oleic acid (OA; Aldrich, tech., 90%) were dissolved in 7.9 g of squalene (Fluka, >97%). The reaction mixture was purged by a stream of argon for 1 h at 150 °C and then at 175 °C for an additional hour. Thereafter, the mixture was heated to the appropriate temperature (230−300 °C), at a heating rate of approximately 20 °C/min and the sample was kept at that temperature for 1 h. After being cooled to room temperature, the sample was washed 4−5 times by sequential magnet-assisted precipitation and redispersion in toluene.

Characterization. HRTEM and energy-dispersive X-ray analysis (EDX) were performed using Philips CM-20 and JEOL JEM 2010F microscopes, both operating at 200 kV. Samples for electron microscopy were prepared by drop-casting of a dilute solution of the nanoparticles in toluene, on 400-mesh carbon-coated copper grids and quickly removing the excess of solution. XPS characterization was performed using a VG Escalab 250 iXL ESCA instrument (VG Scientific). The XPS measurements were carried out using monochromatic Al-Kα radiation ($h\nu$ = 1486.92 eV), photoelectrons were collected at a takeoff angle of 90 °C relative to the sample surface, in constant analyzer energy (CAE) mode, with a 100 eV pass energy for survey spectra and 20 eV pass energy for high-resolution spectra. The C1s charge was calibrated by setting the C1s photopeak to 285.0 eV (the C1s hydrocarbon peak). AFM/MFM images were collected with a Veeco Multimode and a Nanoscope V controler using Veeco RTESP (silicon nitride) tips for AFM and MESP (chromium and cobalt coated) tips for MFM, with a respective resonance frequency of 286.2 kHz and 78.6 kHz and respective spring constants of k = 20−80 N/m and k = 1−5 N/m. In MFM, the quality factor was optimized and calculated for the thermal spectra at $Qf > 1800$. The interleave lift mode distance was set to 100 nm and the scan rate to 0.501 Hz. Field and temperature dependent magnetic measurements were performed on an assembly of the iron oxide nanooctahedra with an edge length of approximately 48 nm, which are shown in Figure 1 after drying a 50 μL drop on a Si substrate, using a commercial SQUID magnetometer in the temperature range 5 K ≤ T ≤ 370 K and a magnetic field up to 5 T. During all measurements the magnetic field was applied in the substrate plane.

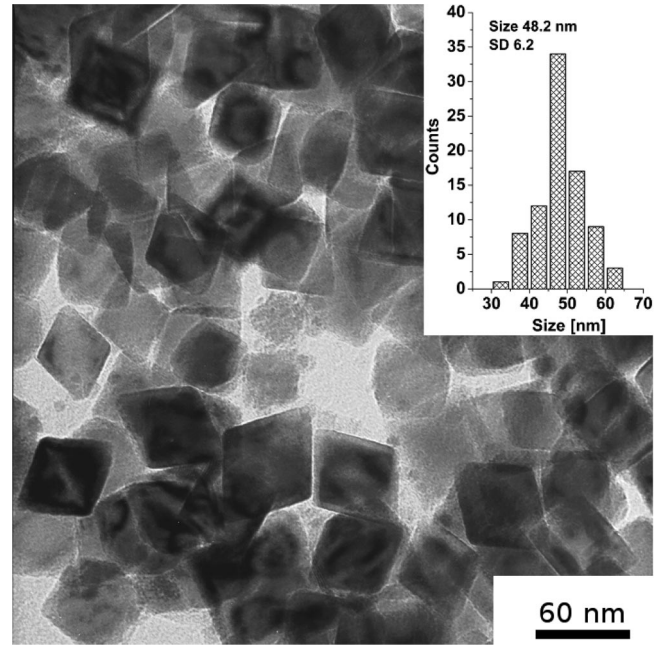

Figure 1. Representative TEM image of iron oxide nanooctahedra obtained by iron oleate decomposition in the presence of TOAB (see Figure 3 for high-resolution images).

Results and Discussion

The formation of iron oxide nanocrystals takes place through thermolytic decomposition of iron oleate in a suitable organic solvent, for example octadecene, paraffin oil or squalene. The use of surfactants that may undergo chemical transformations during the reaction have been recently shown to assist the formation of nanocrystals with faceted morphologies (see for example ref 2 and 3, where both sodium and potassium oleates were used for the efficient preparation of iron oxide nanoparticles with cubic shape). Oleates of alkaline metals (in particular K and Na) dissociate at high temperature (about 200 °C) in organics, producing oleate anions which can act as shape

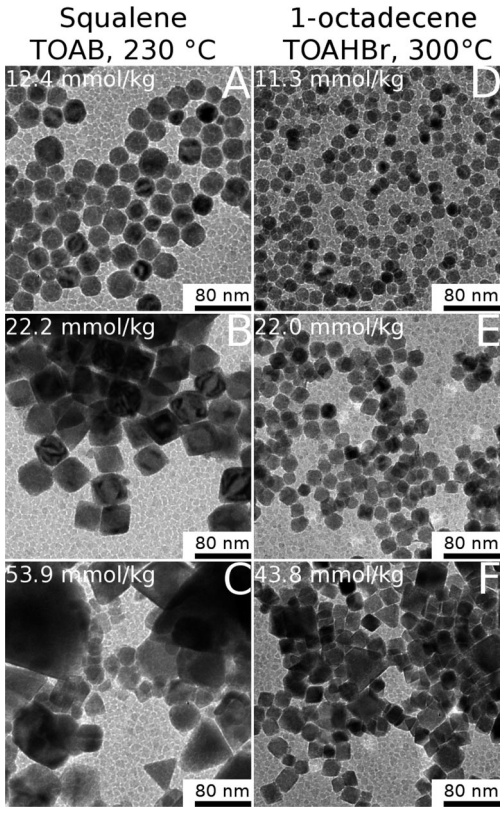

Figure 2. Influence of TOAB (left) and TOAHB (right) on the shape of iron oxide nanocrystals. The concentrations of the corresponding additives are indicated within each TEM image. The synthesis was carried out under different conditions regarding solvent and temperature, intending to show that shape depends only on chemical additives.

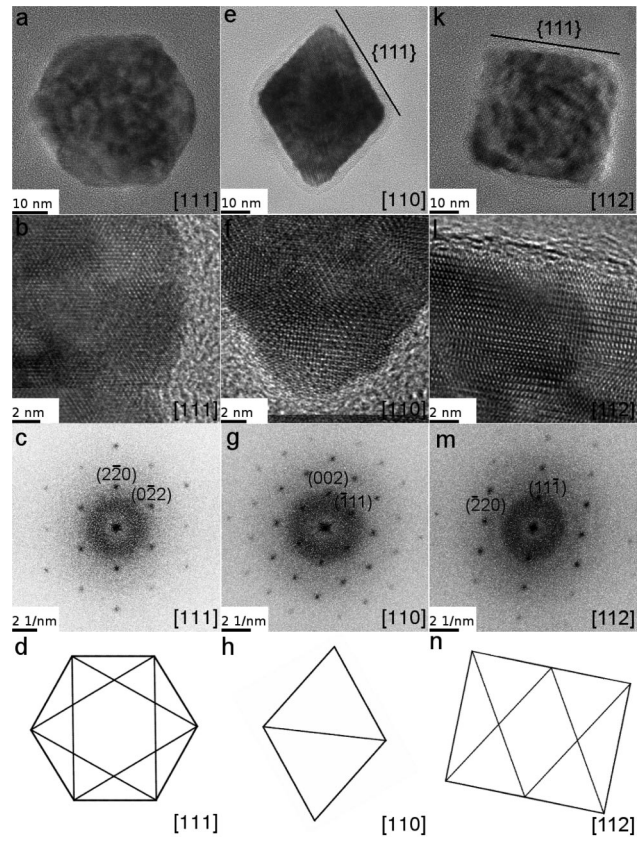

Figure 3. TEM images of a single particle from the sample shown in Figure 1, in the (a−c) [111], (e−g) [110], and (k−m) [112] zone axes. (b, f, l) HRTEM images; (c, g, m) corresponding Fourier transform patterns; and (d, h, n) schematic drawings of the octahedron projections.

directing agents. We have observed that the reaction temperature has some influence on particle size, rather than on the shape of nanooctahedra (see Figure 2), but a detailed study is out of the scope of this paper. We report herein the influence of a different kind of charged surfactants (quaternary ammonium salts) on the shape of iron oxide nanocrystals. We have observed that the addition of small amounts of tertraoctylammoium bromide (TOAB) leads to a drastic change in the shape of the obtained nanoparticles, ultimately allowing the preparation of iron oxide nanocrystals with octahedral shape, as exemplified in Figure 1 through a representative TEM image. In the inset of the same figure, we plotted an indicative size distribution for this sample. An estimate of the particle size was obtained using a circumradius (the minimum radius of a circumference inside which the nanocrystal projection can be fully embedded), because the different orientations of the nanooctahedra might easily lead to misunderstanding (see Figure S1 in the Supporting Information for details).

It is well-known that quaternary ammonium salts are thermally unstable and can undergo several transformations upon heating. Scheme 1 shows various of the possible reactions that can be thermally induced on tetraoctylammonium bromide (TOAB). At elevated temperatures, quaternary ammonium halides can decompose into the corresponding tertiary amine and bromoalkane[9−11] (Scheme 1B), but the cation can also be attacked by the bromine anion yielding an amine, an alkene and HBr (Hoffman elimination, Scheme 1A). Additionally, bromoalkanes (the product of reaction B) can decompose into HBr and the corresponding alkene (Scheme 1C). Finally, HBr (a product in reactions A and C) can react with amines to yield the corresponding salt (Scheme 1D).

As a result of these reactions, three main compounds can be present in the solution: trioctylamine (TOA), trioctylammonium bromide (TOAHB) and TOAB (we cannot completely exclude the possibility of incomplete TOAB decomposition). We can however exclude the presence of pure HBr due to the high probability of the recombination reaction between the amine and HBr or to its elimination with the running Ar flow. Several reactions were carried out to evaluate the influence of the various products of TOAB thermal decomposition on the shape of the resulting nanoparticles. First of all, the presence of pure TOA in any concentration (either addition of small amounts or using it as a solvent) has not been observed to influence the shape of the obtained iron oxide nanocrystals (see Figure S2 in the Supporting Information). We have discarded the influence of octyl bromide and 1-octene because they have relatively low boiling points (201 and 123 °C, respectively), which are well below the reaction temperatures. Taking into account

(9) Sawicka, M.; Storoniak, P.; Blazejowski, J.; Rak, J. *J. Phys. Chem. A* **2006**, *110*, 5066–5074.
(10) Prasad, M. R. R.; Krishnan, K.; Ninan, K. N.; Krishnamurthy, V. N. *Thermochim. Acta* **1997**, *297*, 207–210.
(11) Lubkowski, J.; Blazejowski, J. *Thermochim. Acta* **1990**, *157*, 259–77.

Scheme 1. Possible Reactions in the Reaction Mixture, Leading to the Decomposition of Quaternary Ammonium Salts

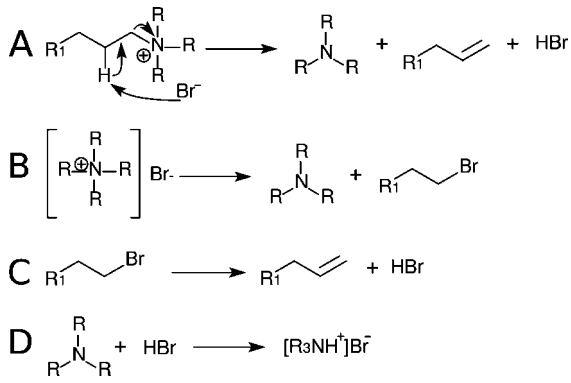

Scheme 2. Schematic Drawing of the Octahedral Shape of the Nanocrystals in Perspective, With Indication of the Main Zone Axes; All Outer Faces of the Octahedron Are {111} Magnetite Facets

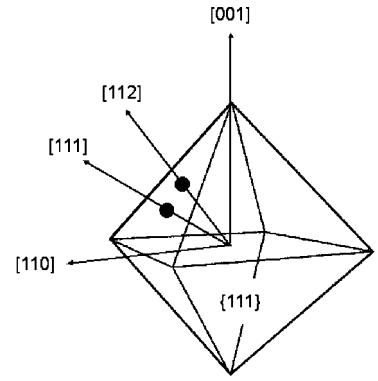

that a constant flow of argon was maintained during the reaction, we can conclude that most probably (it is difficult to make a detailed analysis of the reaction mixture during reaction) both compounds are removed with the argon flow. An additional argument against the influence of 1-octene on the particle shape is the chemical similarity with the standard solvents used (1-octodecene, squalene, octylether, etc). Therefore, we concluded that the only compounds of interest were TOAB and TOAHB. Another imporatant factor that can influence the shape of iron oxide nanoparticles is water.[12] In our case, water can basically enter the synthetic mixture only as contamination from air or from the commercial chemicals used. However, iron oleate was thoroughly dried under a flow of argon at 120 °C and the whole reaction mixture was dried additionally by a flow of Ar during 1 h at 150 °C and for an additional hour at 175 °C. Thus, we do not think what the water content is significant so as to play an important role at our synthetic conditions.

To study the influence of the amount of TOAB and TOAHB in the synthesis, we carried out two sets of experiments. The TEM images in Figure 2 reflect the evolution of the shape of the obtained nanocrystals, as a function of the added amount of TOAB and TOAHB using squalene and 1-octadecene as solvents, respectively. The concentration of the iron precursor was fixed at 0.11 mmol/kg. It is clear that increasing the TOAB concentration from 0 up to 53.9 mmol/kg leads to a dramatic shape transformation, from spheres to octahedra. It can be observed that the system is extremely sensitive to the added amount of TOAB. It is, however, difficult to establish an optimal concentration; high-quality octahedra could only be prepared within a narrow concentration range. As mentioned above, the optimal TOAB concentration can also depend on the quality of the solvent.

To check the importance of the trioctylammonium bromide, we carried out a control experiment in which TOAB was synthesized in situ (see the Supporting Information for details). The corresponding amounts of TOA and HBr (48% aqueous solution) were placed in a four-neck flask, and several minutes later the mixture became of a solid because TOAHB formation. Upon completion of the reaction, the iron precursor, oleic acid, and the solvent were added and the synthesis was carried out as usual. Figure S3 in the Supporting Information shows a TEM image of the obtained nanoparticles that exhibit octahedral shape, though often with truncated tips that may be due to the presence of water in the reaction mixture.

Detailed analysis of transmission electron microscopy (TEM) images provided us with additional information about the structure and composition of the nanooctahedra, as shown in Figure 3. This figure illustrates the projected shapes when the nanocrystals are oriented along three different zone axes of the magnetite crystalline lattice (ICSD No. 84611), as well as their high-resolution (HRTEM) images and the corresponding Fourier transform patterns. It should be noted that the spots are rather wide, as previously observed for $Fe@Fe_3O_4$ nanocubes.[3] In the same figure, we have included drawings of the projections of a regular octahedron in the various zone axes, in correspondence with the perspective drawing in Scheme 2, which closely resemble the experimental TEM (projection) images. The HRTEM images in the three different orientations (Figures 3b,f,l) show internal contrast differences, which may be due to the presence of iron metal, or to defects in the characteristic structure of magnetite. Unfortunately, we have not been able to unambiguously identify any of these features. We can also see some surface roughness, but the {111} facets are still maintained as the octahedrons' outer faces.

On the basis of all this structural information, we can conclude that the particles are indeed regular octahedra limited by {111} facets. The crystalline structure corresponds to single crystals, according to the Fourier transform spot patterns, but the width of the spots may indicate the existence of defects or some type of nanostructured interior, in agreement with the contrast differences observed in the low-magnification TEM images. In particular, the image in Figure 3k points toward a core−shell structure, but we could not find any spot, or set of spots, that allowed us to differentiate the core from the shell by Fourier transform filtering. We assume however, that some type of core−shell structure must be present, with a magnetite envelop containing metallic iron islands in its interior. This could also justify the width of the spots. Finally, we should also take into account, as usual

(12) Hofmann, C.; Rusakova, I.; Ould-Ely, T.; Prieto-Centurion, D.; Hartman, K. B.; Kelly, A. T.; Luttge, A.; Whitmire, K. H. *Adv. Funct. Mater.* **2008**, *18*, 1661–1667.

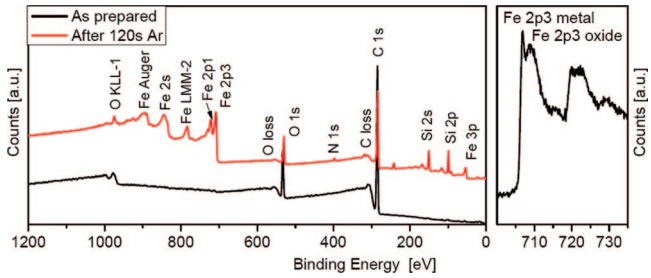

Figure 4. Survey XPS spectrum of iron oxide nanooctahedra, with assignment of the peaks to the corresponding elements (left) and high-resolution spectrum of the Fe2p region (right).

in these systems, that it is very hard (almost impossible) to distinguish between maghemite and magnetite based on the HRTEM investigation.

Figure 4 (left panel) shows survey XPS spectra of the octahedra before and after etching with argon ions. Before etching, the iron signals (either metal or oxide) are basically negligible, because of the presence of a thick organic layer (the capping molecules) on the surface of the nanocrystals. However, after 120s of etching by argon ions, we were able to obtain clear signal of metallic iron inside the ocahedra (Figure 4, right panel). The average Fe^0 content was 14.9 at. % (assuming a random distribution and orientation of the nanoparticles on the substrate). These results seem to confirm the presence of two different magnetic phases, in agreement with the TEM results, and were confirmed by magnetic measurements as described below.

Atomic force microscopy (AFM) analysis provided complementary characterization of this system. Representative images are shown in Figure 5, which reveals the uneven distribution of the particles on a polyelectrolyte-coated surface (poly(styrene sulfonate), PSS). The tapping mode (TM) height image shows the presence of aggregates together with a few isolated particles, whereas the phase image zoom (Figure 5B) allows us to distinguish few octahedra, typically with well-defined triangular facets, corresponding to the most stable orientation of the octahedra on the substrate. A closer look at individual nanocrystals provided uniform profiles (see Figure S4 in the Supporting Information for details). Typical results of additional magnetic force microscopy (MFM) characterization are shown in Figure 5C−E, where a topography image, is compared to the magnetic phase (interleave lift height of 100 nm) and the normal phase image. It should be noted that the magnetic phase intensity results cannot be considered to be quantitative measurements because the principle of MFM is to measure a phase change in the resonance frequency spectrum of the (magnetized) cantilever, compared to the original resonance frequency while scanning different regions of the sample. Consequently, the z scale of the image is indicative only of a contrast difference between the polyelectrolyte surface and the iron oxide particle that gives the magnetic signal. Because the particles are small and sometimes packed as disordered multilayers on the surface, magnetic domains could not be observed in the MFM phase images. However, we do see that all the particles show a black contrast in the magnetic phase image, indicating that the spins are either all upward or all downward.

Figure 6 shows the zero-field-cooled (ZFC) and field-cooled (FC) sample magnetization as a function of temperature. For ZFC measurement, the sample was cooled in zero external magnetic field from 370 K down to 5 K, then a magnetic field of 10 mT was applied and the magnetization was measured with increasing temperature. For FC measurements, the sample was cooled in a magnetic field of 10 mT from 370 to 5 K, and the magnetization was measured at 10 mT while the temperature increased.

The ZFC curve increases nonmonotonically with increasing temperature, and shallow maxima can be distinguished at approximately 105 and 230 K. The FC magnetization shows a clear maximum at 225 K. Over the whole temperature range, the FC curve yields a larger magnetization and approaches the value of the ZFC magnetization above 370 K. This complex magnetic response is due to the contribution from several magnetic phases with different magnetic anisotropy energy. Contribution from different phases is also reflected in the shape of the hysteresis loops measured at 5 and 300 K (Figure 7).

The hysteresis loop recorded at 5 K has a narrowing at low fields and larger hysteresis at higher fields. At 5 K we find a coercive field $\mu_0 H_c = 80$ mT and a high irreversibility field $\mu_0 H_{ir} = 3$ T. $\mu_0 H_{ir}$ is the magnetic field at which both branches of the hysteresis loop merge into a single curve. High irreversibility field shows that some of the nanoparticle spins have a "switching field" of 3 T, indicating the presence of a spin-glass-like, disordered magnetic phase that has been shown to exist at the surface of iron oxides and at the interfaces between Fe and iron oxide.[3] The low-field narrowing of the magnetic hysteresis might be observed in a sample comprising several ferromagnets with different anisotropy energies. However, contribution from a superparamagnetic phase would lead to the same effect. It should be noted that narrowing of the magnetic hysteresis is expected in the case that there is no exchange interaction between the magnetic particles. Otherwise, in the mixture of magnetically hard and magnetically soft phases the "exchange-spring" like behavior would be observed.[13] Because the particles in our sample are spatially separated by a surfactant, no significant exchange interaction is expected.

At 300 K, the field dependent magnetization shows hysteresis with a coercive field $\mu_0 H_c = 10$ mT and an irreversibility field $\mu_0 H_{ir} = 0.1$ T. At both temperatures, the magnetization of the nanocrystal assembly is not saturated at a field of 5 T. A small decrease of 4.5% in the sample magnetization measured at 5 T was observed when the sample was heated from 5 K up to 300 K. The ratio of the remanent magnetization to the magnetization measured at 5 T is equal to 0.2 at 5 K and 0.09 at 300 K. These low values for the remanent to high-field magnetization ratio indicate the presence of superparamagnetic and/or paramagnetic phases. The presence of different magnetic phases within individual particles is also responsible for the observed exchange bias effect: the hysteresis loop of the particle assembly that has been cooled to 5 K from 370 K under a static magnetic field of 5 T is shifted along the field axis in the opposite direction to the cooling field (Figure 8).

(13) Kneller, E. F.; Hawig, R. *IEEE Trans. Magn.* **1991**, *27*, 3588–600.

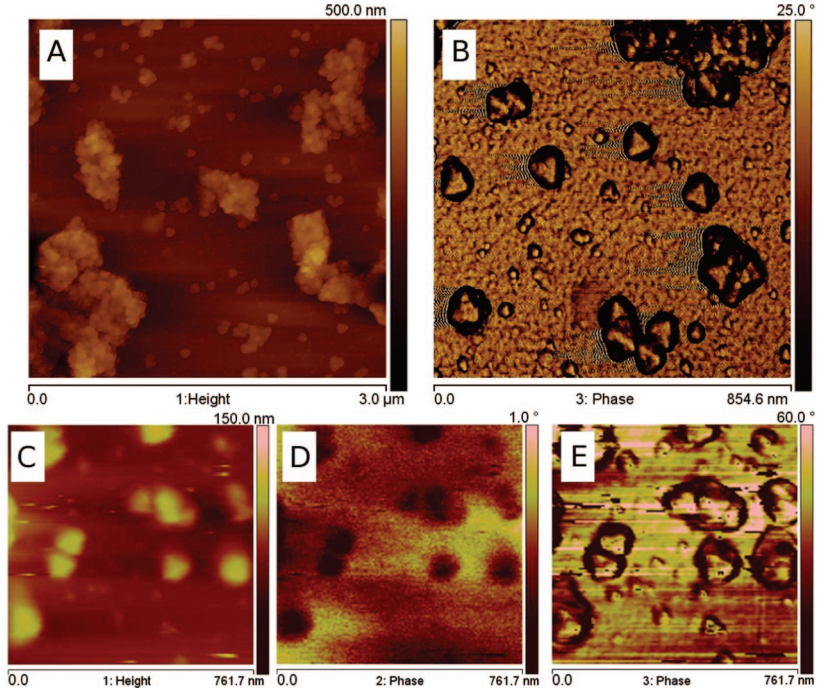

Figure 5. AFM/MFM images of iron oxide octahedra: (A) height 3 × 3 μm image, (B) phase representation, (C) at 100 nm interleave lift scan height, (D) magnetic phase given by the interleave representation, and (E) normal phase.

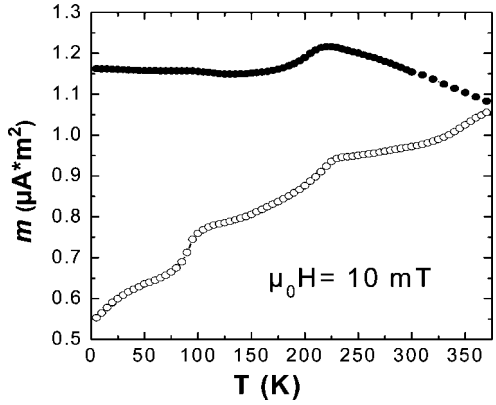

Figure 6. Temperature dependence of the ZFC (open symbols) and FC (filled symbols) magnetization of the assembly of iron oxide nanooctahedra.

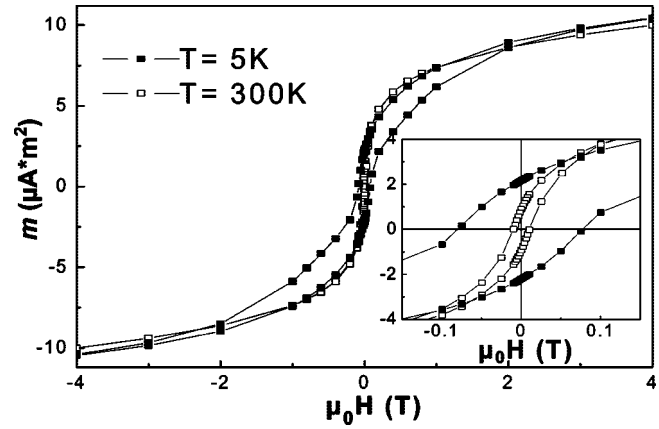

Figure 7. Hysteresis loops for iron oxide nanooctahedra with an edge length of 48 nm, recorded at 5 K (filled symbols) and 300 K (open symbols). The inset shows the low-field part of the magnetic hysteresis loops.

The value of the exchange bias field ($\mu_0 H_{eb}$) is estimated from the shift of the center of the magnetization loop in the field axis. The measured values of $\mu_0 H_{eb}$ and the coercive field ($\mu_0 H_c$), at 5 K after field cooling, are 130 mT and 180 mT, respectively, whereas the ZFC hysteresis loop is symmetrical around the origin with $\mu_0 H_c = 80$ mT. Hence, field-cooling seems to result in an induced unidirectional anisotropy (shift of the hysteresis loop or exchange bias), as well as increased uniaxial magnetic anisotropy, which results in broadening of the hysteresis loop. Exchange bias is a phenomenon associated with an induced exchange anisotropy at the interface between ferromagnetic and antiferromagnetic phases in a heterogeneous system.[14−18] In addition to the exchange bias at the ferromagnetic/antiferromagnetic interfaces, exchange bias has been observed for different systems with glassy magnetic behavior such as ferromagnetic/spin glass core/shell particles[3,19] and intrinsically phase separated cluster-glass compounds.[20,21]

The physical origin of the exchange bias is the exchange coupling between the ferromagnetic and antiferromagnetic or frustrated glassy spins at the interface. During field cooling, the interface antiferromagnetic and ferromagnetic spins align ferromagnetically. An additional torque on ferromagnetic moments, originating from the coupling between these interfacial spins, has to be overcome by an external magnetic field. In the case when the antiferromagnetic anisotropy is larger than the interfacial exchange interaction, the shift of the hysteresis loop, which is due to the presence of a magnetic phase whose moments cannot be reversed by the applied field, is observed. When the strength of the exchange anisotropy interaction is comparable to that of the

(14) Meiklejohn, W. H. *J. Appl. Phys.* **1962**, *33*, 1328–35.
(15) Nogués, J.; Schuller, I. K. *J. Magn. Magn. Mater.* **1999**, *192*, 203–232.
(16) Berkowitz, A. E.; Takano, K. *J. Magn. Magn. Mater.* **1999**, *200*, 552–570.

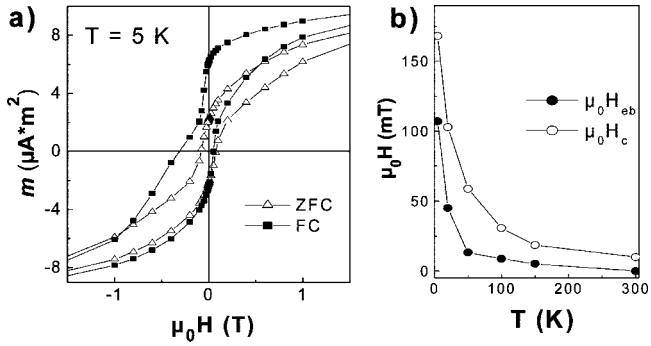

Figure 8. (a) Hysteresis loops of the iron oxide nanooctahedra recorded at 5 K after cooling the sample in a magnetic field of 5 T (FC, filled symbols) and in a zero field (ZFC, open symbols). (b) Exchange bias field, H_{eb}, and coercive field, H_c, as a function of temperature for 48 nm iron oxide nanooctahedra after FC in 5 T.

antiferromagnetic anisotropy, broadening of the hysteresis loop is observed because of the contribution of a reversible interfacial phase.[17,22] We have simultaneously observed the shift and broadening of the hysteresis loop, which indicates a local variation of antiferromagnetic anisotropy energy and/or interfacial exchange interaction. In addition, we have observed a vertical shift of the FC hysteresis loop: the sample magnetization measured at 5 T is 17% larger in the cooling field direction than in the heating direction. This is due to the presence of pinned ferromagnetic spins, which cannot be reversed by a magnetic field of 5 T. Small iron clusters in an iron oxide matrix can be considered as a source of such spins. The magnetic hysteresis was measured at different temperatures during heating of the FC sample. We plotted in Figure 8b the temperature dependence of both the exchange bias and coercive field. The exchange bias field decreases with increasing temperature and completely vanishes above 150 K. At this temperature, thermal disorder becomes dominant over the induced magnetic unidirectional anisotropy.

Conclusions

High-quality iron oxide nanooctahedra were synthesized by thermolysis of iron oleate in the presence of tetraoctylammonium bromide. Quaternary ammonium salts can undergo various chemical reactions yielding trioctylammonium bromide, which plays an important role on the determination of the shape of the obtained nanoparticles. Detailed HRTEM studies were carried out, demonstrating that the particles are regular octahedra limited by {111} facets. The crystalline structure corresponds to single crystals, according to the Fourier transforms from the HRTEM images, but the width of the spots may indicate the existence of inner defects. From this and other characterization techniques, the material comprising these particles was identified as magnetite with islandlike areas of metallic iron in its interior. This was also related to the measured complex magnetic response, which arises from the contribution of several magnetic phases with different magnetic anisotropy energies. Magnetic inhomogeneity within individual particles is reflected in field-cooling- induced effects, such as exchange bias, broadening of the magnetic hysteresis, as well as a vertical shift of the magnetization loop.

Acknowledgment. This work was supported by the European Community's Marie-Curie Research Training Network "SyntOrbMag" (Contract MRTN-CT-2004-005567), the Xunta de Galicia and the Spanish Ministerio de Ciencia e Innovación through the project "Nanobiomed (CONSOLIDER-INGENIO 2010)". The authors are thankful to Dr. Carmen Serra (CACTI, U. Vigo) for performing XPS measurements and to Dr. Sergei Voitekhovich, Dr. Gema Antequera García, and Dr. Carlos Pérez Balado for useful discussion and expertise in chemistry of organic compounds.

Supporting Information Available: Additional figures (PDF). This material is available free of charge via the Internet at http://pubs.acs.org.

CM803201P

(17) Nogués, J.; Sort, J.; Langlais, V.; Skumryev, V.; Suriñach, S.; Muñoz, J.; Baró, M. *Phys. Rep.* **2005**, *422*, 65–117.
(18) Nogués, J.; Sort, J.; Langlais, V.; Doppiu, S.; Dieny, B.; Muñoz, J. S.; Suriñach, S.; Baró, M. D.; Stoyanov, S.; Zhang, Y. *Int. J. Nanotechnol.* **2005**, *2*, 23–42.
(19) Martinez-Boubeta, C.; Simeonidis, K.; Angelakeris, M.; Pazos-Perez, N.; Giersig, M.; Delimitis, A.; Nalbandian, L.; Alexandrakis, V.; Niarchos, D. *Phys. Rev. B:* **2006**, *74*, 054430/1–054430/10.
(20) Thakur, M.; Patra, M.; De, K.; Majumdar, S.; Giri, S. *J. Phys.: Condens. Matter* **2008**, *20*, 195215/1–195215/5.
(21) Tang, Y.-k.; Sun, Y.; Cheng, Z.-h. *Phys. Rev. B.* **2006**, *73*, 174419/1–174419/6.
(22) Soeya, S.; Nakamura, S.; Imagawa, T.; Narishige, S. *J. Appl. Phys.* **1995**, *77*, 5838–42.